T2WI-BCMIC: Non-Fat Saturated T2-Weighted Imaging Dataset for Bladder Cancer Muscle Invasion Classification

Han Huang[1*], Weiyi Chen[1*], Qiuxia Wu[1†], Huanjun Wang[2], Qian Cai[2], and Yan Guo[2]

[1] South China University of Technology
[2] The First Affiliated Hospital, Sun Yat-Sen University

Abstract. Accurate classification of muscle invasion in bladder cancer using computer-aided diagnosis (CAD) is crucial for timely intervention and improved prognosis. Despite advances in deep learning for medical image analysis, muscle invasion classification remains limited by the scarcity of publicly available annotated datasets. To address this, we introduce T2WI-BCMIC, the first expert-annotated dataset for bladder cancer muscle invasion classification. T2WI-BCMIC contains Non-fat saturated T2-weighted magnetic resonance imaging (MRI) images with five-class annotations, covering various invasion depths. We establish a benchmark using several popular deep learning architectures, providing a solid foundation for future comparisons. However, achieving further performance improvements remains challenging due to the small dataset size. Therefore, we propose a novel search-based data augmentation algorithm that increases data diversity by maximizing the divergence from the class-specific manifold, while preserving the class distribution to maintain class identity. Experimental results on T2WI-BCMIC show that our algorithm outperforms existing methods, achieving significant performance improvements. The T2WI-BCMIC dataset and benchmark are available at: https://github.com/T2-MI/T2WI-BCMIC for further research.

Keywords: Bladder cancer dataset · Deep learning · Data augmentation.

1 Introduction

Bladder cancer, a significant urinary malignancy, ranks among the top 10 global cancers, with approximately 500,000 new diagnoses and 200,000 deaths per year [24,21,26]. Muscle invasion risk assessment is crucial for diagnosis, treatment planning, and prognosis in bladder cancer [15]. While MRI is increasingly employed for this purpose, manual clinical interpretation is hindered by scarce

*Equal contribution, †Corresponding author: qxwu@scut.edu.cn.

expert availability, clinician fatigue, and inter-observer variability, reducing assessment efficacy. Improving the accuracy of muscle invasion risk stratification is therefore essential for better clinical outcomes.

To mitigate the limitations of manual assessment and advance muscle invasion risk stratification, inherently a computer vision classification problem, CAD is garnering increasing research interest. While CAD has progressed significantly in medical image analysis, encompassing lesion classification [35,25,1], detection [23,8,13], and segmentation [6,2,11], muscle invasion classification in bladder cancer remains relatively under-explored. Current bladder cancer image datasets predominantly address tissue classification or segmentation, as detailed in Table 1, tasks distinct from muscle invasion risk assessment. A major barrier to progress is the lack of publicly available, annotated datasets for muscle invasion classification, which hampers research and clinical translation. Creating such datasets demands substantial clinical expertise [16] and faces challenges like data privacy concerns, restricted access [29,7], and other obstacles, contributing to the scarcity of public resources.

Table 1. Bladder medical image datasets available publicly, including multi-organ datasets from TCIA (The Cancer Imaging Archive).

Dataset	Source	Task
Crowds-Cure-2018 [30]	TCIA	Segmentation
CT-ORG [22]	TCIA	Segmentation
Pan-Cancer-Nuclei-Seg [10]	TCIA	Segmentation
T24	The Cancer Cell Institute at the University of Cambridge	Segmentation
Bladder MRI Segmentation Dataset (2018)	2018 China University Computer Design Competition	Segmentation
Bladder MRI Segmentation Dataset (2019)	2019 International Symposium on Image Computing and Digital Medicine	Segmentation
EBTC [14]	DataCite Commons	Classification

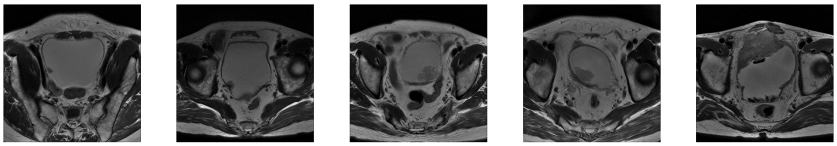

Fig. 1. Examples from the T2WI-BCMIC dataset, illustrating five-class annotations.

Deep neural networks (DNNs) have demonstrated remarkable efficacy in medical image classification [35,25,1]. However, their reliance on large datasets con-

trasts sharply with the scarcity of labeled medical data, often leading to overfitting. Data augmentation is a common solution, but conventional methods like rotation and flipping are low-level, data-independent, and distribution-agnostic operations [31,4], offering limited diversity and potentially distorting the true data distribution. To address these shortcomings, we propose a novel augmentation algorithm that formulates augmentation as a search process. This approach optimizes augmented samples by maximizing their divergence from the class-specific manifold of original samples while preserving the inherent distribution of the class, thereby enhancing both diversity and consistency.

To address the dataset gap in bladder cancer muscle invasion classification, we introduce T2WI-BCMIC, a novel T2-Weighted Imaging (T2WI) dataset. Comprising 353 DICOM images with five-class VI-RADS [20] annotations, T2WI-BCMIC is publicly released. Fig 1 illustrates example images and annotations. We benchmark several popular deep learning approaches on T2WI-BCMIC to establish a performance baseline and demonstrate the challenges of muscle invasion classification in clinical settings. Furthermore, we evaluate our data augmentation algorithm's effectiveness in improving muscle invasion classification performance across several different network architectures using our dataset.

In summary, our main contributions are:

- We introduce the first publicly available multi-class dataset specifically designed for muscle invasion risk classification in bladder cancer, addressing a critical gap in current research and providing a valuable resource for the community.
- We perform a comprehensive benchmark evaluation of widely-used DNNs on the T2WI-BCMIC dataset, establishing a robust performance baseline to guide future studies in this domain.
- Leveraging the T2WI-BCMIC dataset, we propose a novel search-based augmentation algorithm tailored for bladder cancer image analysis, which overcomes the limitations of traditional augmentation methods and significantly enhances classification performance.

2 T2WI-BCMIC Dataset

The T2WI-BCMIC dataset is created to address the lack of data for bladder cancer muscle invasion classification, offering the first publicly available multi-class dataset for this purpose. It ensures balanced representation across the five VI-RADS categories [20], facilitating unbiased model development.

2.1 Data Collection

Table 2 summarizes the key parameters for data acquisition and the characteristics of the T2WI-BCMIC dataset. The dataset is predominantly male (age range 40-85 years) and reflects the demographics of patients undergoing clinical muscle invasion assessment. Detailed age and gender distributions are provided in the supplementary materials.

Table 2. Overview of the T2WI-BCMIC, including key characteristics and imaging protocols.

Item	Details	Comments
Number of Images	335 Non-Fat T2WI	
Number of Cases	159 patients	Male-biased, higher male incidence
Gender Distribution	3.7:1 male-to-female	Consistent with male prevalence
Age Range	40 to 85 years	Typical age range
Risk Categories	5 categories	VI-RADS based
Collection Period	2013-2023	Ten-year collection
Imaging Equipment	3.0T MRI	High-resolution imaging
Sample Source	the First Affiliated Hospital, Sun Yat-Sen University	Clinically reliable data
Scanning Protocol	T2-weighted PROPELLER	Optimized for bladder cancer

Data are retrospectively collected over a ten-year period (2013–2023) from the First Affiliated Hospital, Sun Yat-Sen University, a leading medical center, with ethical approval granted by the hospital's Ethics Committee. All images are anonymized to ensure patient privacy. Imaging is conducted using a 3.0T MRI system (Signa Pioneer, GE Healthcare) with a 32-channel body coil. Patients follow a standardized preparation protocol, including voiding two hours prior to the MRI and refraining from urination and fluid intake until completion. The imaging protocol employe an axial T2-weighted PROPELLER sequence with the following parameters: TR/TE = 4817/125.7 ms, slice thickness = 4 mm, FOV = 220 mm, acquisition matrix = 320, and NEX = 3.

2.2 Dataset Annotation

All samples are annotated by a team of seasoned radiologists using the VI-RADS criteria to assess the risk of bladder cancer invasion. Three physicians, each possessing at least five years of experience, contribute to the annotation process, analyzing a maximum of 30 images per week to ensure annotation accuracy.

3 Method

This section presents a search-based algorithm for bladder image augmentation, consisting of three core components: the Constrained Optimization Model (COM) for setting optimization criteria, the Keypoint Detection Module (KPDM) for identifying anatomical key points, and the Augmented Data Search Module (ADSM) for optimizing key point transformations to create diverse augmented samples. These modules work together to balance data diversity enhancement with class identity preservation, as illustrated in Fig 2.

3.1 Constrained Optimization Model (COM)

To address the limitations of conventional augmentation methods, our algorithm employs a constrained optimization model for bladder image augmentation, in-

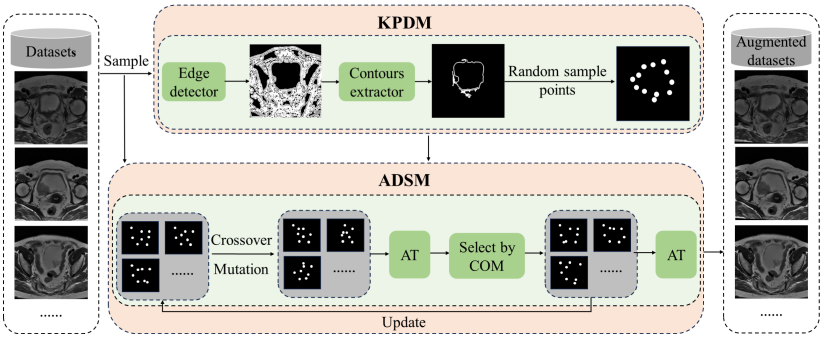

Fig. 2. Bladder image data augmentation algorithm based on constrained optimization using affine transformation (AT).

tegrating the KPDM and ADSM modules. The overarching approach maximizes the divergence between augmented images (x') and the original data distribution to enhance data diversity, while ensuring that each augmented image (x') effectively retains the class identity of its corresponding original image (x).

The optimization problem is mathematically formulated as:

$$\begin{aligned} \textbf{max} \quad & \mathcal{R}(x') = \sum_{i=1}^{k} \lambda_i \left(\sum_{j \in \mathcal{N}(x')} \hat{w}_{ij} \mathbf{V}_{ji} \right)^2 \\ \textbf{subject to} \quad & x' = Aug(x) \\ & x \in D_c, \\ & \text{softmax}(\text{logits}(x'))_c = \text{softmax}(\text{logits}(x))_c \\ & \quad \text{or} \quad \text{logits}(x')_c \geq \text{logits}(x)_c \end{aligned} \tag{1}$$

In this formulation, the ADSM searches for augmented samples (x') that maximize the divergence from the original data manifold, as measured by the Manifold Regularization Score $\mathcal{R}(x')$, which quantifies how poorly the augmented samples align with the underlying low-dimensional manifold of the original data. This score is computed using top-k Laplacian eigenvalues (λ_i) and neighborhood contributions ($\mathbf{V}_{ji}$, weighted by $\hat{w}_{ij}$), learned from a pre-trained model. The ADSM-driven optimization promotes data diversity while ensuring class identity preservation through a broader constraint, either by maintaining softmax probabilities or keeping the logit score for the correct class (D_c is the data set of the corresponding category) in the augmented sample at least as high as in the original.

3.2 Keypoint Detection Module (KPDM)

In the absence of bladder/lesion annotations in the T2WI-BCMIC dataset, the KPDM autonomously identifies key points for image deformation. This mod-

ule integrates an edge detection algorithm [33] with geometric priors to detect relevant key points in the bladder. Initially, an edge detection algorithm is applied to delineate boundary regions. For each detected contour, the mean pixel intensity u_k within the contour region $\mathcal{C}_k$ is computed (Eq. 2). Contours with an intensity below a predefined threshold ($u_k < u_{\min}$) are excluded to eliminate irrelevant boundaries. Subsequently, geometric properties—such as the area A_k, centroid position C_k, and position bias B_k, which represents the squared L1 distance from the contour's centroid to the image center (Eq. 3)—are calculated. The relevance probability P_k of each contour is then determined by a weighted combination of area and position bias (Eq. 4). These combined steps form the *Contours extractor* in Fig 2. Finally, key points are randomly sampled from the top-k contours, ranked by their relevance probability.

$$u_k = \frac{1}{|\mathcal{C}_k|} \sum_{\mathbf{p} \in \mathcal{C}_k} I(\mathbf{p}) \tag{2}$$

$$B_k = \|\mathbf{C}_k - \mathbf{C}_{\text{image}}\|_1^2 \tag{3}$$

$$P_k = \alpha \cdot A_k + \beta \cdot B_k \tag{4}$$

The method integrates geometric priors with edge detection to reliably identify key points. First, contours are filtered based on pixel intensity, and then ranked using the area and position bias, which reflect their alignment with the image center. The relevance probability guides the selection of the most relevant contours, prioritizing those that are geometrically significant and structurally consistent with the bladder anatomy.

3.3 Augmented Data Search Module (ADSM)

The ADSM integrates constraints to maintain the class identity of augmented samples, ensuring alignment with the original data distribution. By balancing data diversity and class identity preservation, it identifies optimal key point transformations, producing augmented samples that enhance diversity while retaining the original data's inherent characteristics. To effectively address this, the Genetic Algorithm (GA)[18] offers a robust solution. Within this framework, the GA evolves candidate transformations over generations, selecting the best transformations based on manifold regularization scores and class identity preservation. Crossover or mutation create new transformations, which are evaluated in subsequent generations. The process iterates until convergence, producing optimal transformations for generating augmented samples. The pseudocode of the full search process is detailed in the supplementary material.

4 Experiments and Results

We evaluate several widely-used networks and our proposed augmentation algorithm on the T2WI-BCMIC dataset. The experimental details and results, presented below, demonstrate the method's effectiveness.

4.1 Implementation Details

Five-fold cross-validation on T2WI-BCMIC is used to evaluate network performance. Training is performed for 200 epochs with a batch size of 16, utilizing SGD optimization and a weight decay of 5e-4. Initial learning rates are set to 0.1 for DenseNet121, 0.001 for VGG, and 0.01 for other networks. For the augmentation comparative studies, MRI images are preprocessed to an 8-bit integer format ([0, 255]). The augmentation protocol replicates the benchmark setup, with a uniform initial learning rate of 0.001 for all networks. The parameters of GA are as follows: a population size of 100, a crossover probability of 1.0, and a mutation rate of $1/16$ per coordinate, with a total of 16 coordinates. And our method selects three optimal images for expanding the training data. All experiments are conducted with NVIDIA GeForce RTX 3090 GPU.

4.2 Main Results

In the initial phase of our study, we benchmarke several commonly used network architectures: GoogleNet [28], VGG [27], ResNet variants[9,32,5,34], and DenseNet121[12], evaluating their performance based on accuracy and F1-score. As shown in Table 3, the ResNet variants, Res2Net50 and ResNest50, initialized with pre-trained weights from natural image datasets, achieve the highest performance, with the same accuracy of 74.55%. Their excellent performance highlights the effectiveness of transferring features from natural images to medical data for bladder cancer muscle invasion classification. In contrast, GoogleNet and DenseNet121 offer a good trade-off between computational efficiency and performance, while VGG provide stable results at higher parameters.

After benchmarking the initial network performance, we evaluate several conventional and state-of-the-art (SOTA) augmentation methods, comparing their performance against our proposed approach. As shown in Table 4, our method consistently outperforms all evaluated networks. For instance, on GoogleNet, it achieves a accuracy of 76.79% and an F1-Score of 76.70%, with improvements of 11.05% and 12.08% over the baseline, respectively. In contrast, traditional methods such as randomRotation (RR) and Cutout, as well as SOTA techniques like TrivialAugment (TA) and RandAugment (RA), show inferior results. For example, Cutout achieves only 62.13% accuracy and 61.99% F1-Score behind the baseline on GoogleNet, while TA and RA fall behind our method, with accuracies of 68.77% and 68.44%, respectively. These results highlight that existing methods struggle with complex medical images like bladder cancer, while our tailored approach significantly boosts performance for this task.

4.3 Ablation Results

The ablation study in Table 5 confirms the effectiveness of the KPDM and ADSM. Integrating either module individually with Res2Net50, ResNest50, or GoogleNet improves performance over the baseline. KPDM alone boosts accuracy and F1-Score, while ADSM independently also delivers significant gains.

The highest performance is achieved when both modules are combined, underscoring their synergistic effect in enhancing the augmentation method's overall effectiveness.

Table 3. Classification results of different networks (Accuracy and F1-Score in %, Parameters in M, FLOPs in G).

Method	Accuracy	F1-Score	Parameters	FLOPs
VGG16	71.21±6.08	70.89±6.24	165.74	20.27
VGG19	71.65±4.36	71.50±4.24	171.05	25.71
GoogleNet	71.93±5.00	71.08±5.83	6.30	34.28
ResNet18	65.05±3.61	64.30±4.36	11.17	35.70
ResNet32	69.10±6.48	68.38±6.86	20.10	69.62
Res2Net50	**74.55±2.74**	**73.98±3.13**	23.66	5.62
ResNest50	74.55±4.12	73.92±4.31	25.44	7.09
ResNext50	62.42±5.10	62.39±5.74	14.79	49.20
DenseNet121	69.14±5.66	68.80±5.48	6.95	58.10

Table 4. Classification results of different augmentation methods (Unit: %).

Method	Res2Net50		ResNest50		GoogleNet	
	Accuracy	F1-Score	Accuracy	F1-Score	Accuracy	F1-Score
Baseline	70.75±5.01	70.08±5.20	73.87±5.10	73.38±5.33	65.74±3.41	64.62±2.71
RR	73.17±1.78	72.90±1.83	74.57±4.95	74.34±4.67	68.02±4.07	67.80±3.76
Cutout[4]	70.24±5.71	69.72±6.19	74.73±4.28	74.11±4.69	62.13±4.74	61.99±5.14
TA[19]	77.47±4.60	77.29±4.49	75.82±3.82	75.45±3.86	68.77±5.57	68.19±5.64
RA[3]	74.66±3.93	73.92±4.27	75.74±3.78	75.29±3.43	68.44±5.79	66.58±8.71
SA[17]	**78.46±5.20**	**78.02±5.74**	73.87±6.34	73.55±6.57	71.43±8.27	70.98±8.14
Ours	77.63±4.61	77.45±5.17	**80.28±4.22**	**79.61±4.51**	**76.79±6.18**	**76.70±6.15**

Table 5. Classification results of module ablation studies (Unit: %).

Module		Res2Net50		ResNest50		GoogleNet	
KPDM	ADSM	Accuracy	F1-Score	Accuracy	F1-Score	Accuracy	F1-Score
-	-	70.75±5.00	70.08±5.20	73.87±5.10	73.38±5.33	65.74±3.41	64.62±2.71
✓	-	76.61±3.49	76.14±3.53	77.91±3.49	77.18±4.07	73.71±6.74	73.48±6.82
-	✓	77.01±3.77	76.68±3.66	77.27±3.67	77.07±3.82	74.68±5.39	74.14±5.09
✓	✓	**77.63±4.61**	**77.45±5.17**	**80.28±4.22**	**79.61±4.51**	**76.79±6.18**	**76.70±6.15**

5 Conclusion

This paper introduces T2WI-BCMIC, the first publicly available multi-class dataset for bladder cancer muscle invasion risk, comprising 159 patient cases that reflect the natural distribution of the disease, addressing a gap in the field. We benchmark a series of DNNs on this dataset to evaluate their performance. Additionally, recognizing the limitations of traditional data augmentation methods, we propose a novel search-based augmentation algorithm specifically designed for bladder cancer images to increase diversity and maintain consistency. Extensive experiments demonstrate the effectiveness of our approach. Moving forward, We aim to expand the dataset with additional modalities to further advance CAD research for multi-class muscle-invasive bladder cancer classification.

Acknowledgments. This work is supported by National Natural Science Foundation of China (62276103), Innovation Team Project of General Colleges and Universities in Guangdong Province (2023KCXTD002), the Research and Development Project on Key Technologies for Intelligent Sensing and Analysis of Urban Events Based on Low-Altitude Drones (2024BQ010011), the 2023 Special Program for Audit Theory Research, Guangdong Provincial Philosophy and Social Science Planning (GD23SJZ09).

Disclosure of Interests. The authors have no competing interests to declare that are relevant to the content of this article.

References

1. Azizi, S., Mustafa, B., Ryan, F., et al.: Big self-supervised models advance medical image classification. In: Proceedings of the IEEE/CVF international conference on computer vision. pp. 3478–3488 (2021)
2. Chaitanya, K., Erdil, E., Karani, N., et al.: Contrastive learning of global and local features for medical image segmentation with limited annotations. Advances in neural information processing systems **33**, 12546–12558 (2020)
3. Cubuk, E.D., Zoph, B., Shlens, J., et al.: Randaugment: Practical automated data augmentation with a reduced search space. In: Proceedings of the IEEE/CVF conference on computer vision and pattern recognition workshops. pp. 702–703 (2020)
4. DeVries, T.: Improved regularization of convolutional neural networks with cutout. arXiv preprint arXiv:1708.04552 (2017)
5. Gao, S.H., Cheng, M.M., Zhao, K., et al.: Res2net: A new multi-scale backbone architecture. IEEE transactions on pattern analysis and machine intelligence **43**(2), 652–662 (2019)
6. Gao, Y., Zhou, M., Metaxas, D.N.: Utnet: a hybrid transformer architecture for medical image segmentation. In: Medical image computing and computer assisted intervention. pp. 61–71 (2021)
7. Goceri, E.: Medical image data augmentation: techniques, comparisons and interpretations. Artificial Intelligence Review **56**(11), 12561–12605 (2023)
8. Graham, S., Vu, Q.D., Raza, S.E.A., et al.: Hover-net: Simultaneous segmentation and classification of nuclei in multi-tissue histology images. Medical image analysis **58**, 101563 (2019)

9. He, K., Zhang, X., Ren, S., et al.: Deep residual learning for image recognition. In: Proceedings of the IEEE conference on computer vision and pattern recognition. pp. 770–778 (2016)
10. Hou, L., Gupta, R., Van Arnam, J.S., et al.: Dataset of segmented nuclei in hematoxylin and eosin stained histopathology images of 10 cancer types (2019). https://doi.org/10.7937/TCIA.2019.4A4DKP9U, https://doi.org/10.7937/TCIA.2019.4A4DKP9U, [Data set]
11. Hu, Q., Chen, Y., Xiao, J., et al.: Label-free liver tumor segmentation. In: Proceedings of the IEEE/CVF conference on computer vision and pattern recognition. pp. 7422–7432 (2023)
12. Huang, G., Liu, Z., Van Der Maaten, L., et al.: Densely connected convolutional networks. In: Proceedings of the IEEE conference on computer vision and pattern recognition. pp. 4700–4708 (2017)
13. Lal, S., Das, D., Alabhya, K., et al.: Nucleisegnet: Robust deep learning architecture for the nuclei segmentation of liver cancer histopathology images. Computers in biology and medicine **128**, 104075 (2021)
14. Lazo, J.F., Rosa, B., Catellani, M., et al.: Semi-supervised bladder tissue classification in multi-domain endoscopic images. IEEE Transactions on biomedical engineering **70**(10), 2822–2833 (2023)
15. Lenis, A.T., Lec, P.M., Chamie, K., et al.: Bladder cancer: a review. Jama **324**(19), 1980–1991 (2020)
16. Litjens, G., Bandi, P., Ehteshami Bejnordi, B., et al.: 1399 h&e-stained sentinel lymph node sections of breast cancer patients: the camelyon dataset. GigaScience **7**(6), giy065 (2018)
17. Liu, Y., Yan, S., Leal-Taixé, L., et al.: Soft augmentation for image classification. In: Proceedings of the IEEE/CVF conference on computer vision and pattern recognition. pp. 16241–16250 (2023)
18. Mirjalili, S., Mirjalili, S.: Genetic algorithm. Evolutionary algorithms and neural networks: Theory and applications pp. 43–55 (2019)
19. Müller, S.G., Hutter, F.: Trivialaugment: Tuning-free yet state-of-the-art data augmentation. In: Proceedings of the IEEE/CVF international conference on computer vision. pp. 774–782 (2021)
20. Panebianco, V., Narumi, Y., Altun, E., et al.: Multiparametric magnetic resonance imaging for bladder cancer: development of vi-rads (vesical imaging-reporting and data system). European urology **74**(3), 294–306 (2018)
21. Richters, A., Aben, K.K., Kiemeney, L.A.: The global burden of urinary bladder cancer: an update. World journal of urology **38**(8), 1895–1904 (2020)
22. Rister, B., Shivakumar, K., Nobashi, T., et al.: Ct-org: A dataset of ct volumes with multiple organ segmentations (2019). https://doi.org/10.7937/TCIA.2019.tt7f4v7o, https://doi.org/10.7937/TCIA.2019.tt7f4v7o, [Data set]
23. Ryu, J., Puche, A.V., Shin, J., Park, S., et al.: Ocelot: overlapped cell on tissue dataset for histopathology. In: Proceedings of the IEEE/CVF conference on computer vision and pattern recognition. pp. 23902–23912 (2023)
24. Saginala, K., Barsouk, A., Aluru, J.S., et al.: Epidemiology of bladder cancer. Medical sciences **8**(1), 15 (2020)
25. Sarvamangala, D., Kulkarni, R.V.: Convolutional neural networks in medical image understanding: a survey. Evolutionary intelligence **15**(1), 1–22 (2022)
26. Siegel, R.L., Miller, K.D., Wagle, N.S., et al.: Cancer statistics, 2023. CA: a cancer journal for clinicians **73**(1), 17–48 (2023)
27. Simonyan, K., Zisserman, A.: Very deep convolutional networks for large-scale image recognition. arXiv preprint arXiv:1409.1556 (2014)

28. Szegedy, C., Liu, W., Jia, Y., et al.: Going deeper with convolutions. In: Proceedings of the IEEE conference on computer vision and pattern recognition. pp. 1–9 (2015)
29. Upadhyay, A.K., Bhandari, A.K.: Advances in deep learning models for resolving medical image segmentation data scarcity problem: A topical review. Archives of computational methods in engineering **31**(3), 1701–1719 (2024)
30. Urban, T., Ziegler, E., Pieper, S., et al.: Crowds cure cancer: Crowdsourced data collected at the rsna 2018 annual meeting (2019). https://doi.org/10.7937/TCIA.2019.yk0gm1eb, https://doi.org/10.7937/TCIA.2019.yk0gm1eb, [Data set]
31. Wang, Y., Huang, G., Song, S., et al.: Regularizing deep networks with semantic data augmentation. IEEE Transactions on pattern analysis and machine intelligence **44**(7), 3733–3748 (2021)
32. Xie, S., Girshick, R., Dollár, P., et al.: Aggregated residual transformations for deep neural networks. In: Proceedings of the IEEE conference on computer vision and pattern recognition. pp. 1492–1500 (2017)
33. Xu, Z., Baojie, X., Guoxin, W.: Canny edge detection based on open cv. In: 2017 13th IEEE international conference on electronic measurement & instruments. pp. 53–56. IEEE (2017)
34. Zhang, H., Wu, C., Zhang, Z., et al.: Resnest: Split-attention networks. In: Proceedings of the IEEE/CVF conference on computer vision and pattern recognition. pp. 2736–2746 (2022)
35. Zhou, S.K., Greenspan, H., Davatzikos, C., et al.: A review of deep learning in medical imaging: Imaging traits, technology trends, case studies with progress highlights, and future promises. Proceedings of the IEEE **109**(5), 820–838 (2021)